Supplementary material for

A simplified representation of the non-linear NO_x chemistry for interpreting emission signal from space-based NO_2 data

Dien Wu

Correspondence to Dien Wu (dienwu@caltech.edu)

Site	Emission	NO_x chemistry	Inter-parcel mixing	Meteorological fields	Model-TROPOMI slope	RMSE (mean bias) [ppb]
New Madrid, MO (8 of 34 overpasses in JJA)	EPA (hourly)	Yes	Yes	GFS	1.22 (J-D); 1.03 (JJA)	0.14 (-26%)
	EPA (hourly)	Yes	Yes	GFS	1.21 (J-D); 1.03 (JJA) with background subtracted	0.15 (/)
	EPA (hourly)	Yes	Yes	HRRR	1.24 (J-D); 1.05 (JJA)	0.11 (-4%)
	EPA (hourly)	Yes	No	GFS	1.19 (J-D); 1.01 (JJA)	0.13 (-28%)
	EPA (hourly)	No	Yes	GFS	1.77 (J-D); 1.68 (JJA)	0.25 (40%)
	EDGARv6 (monthly)	Yes	Yes	GFS	0.53 (J-D); 0.16 (JJA)	0.14 (-49%)
Thomas Hill, MO (9 overpasses in JJA)	EPA (hourly)	Yes	Yes	GFS	1.13 (JJA)	
	EPA (hourly)	Yes	No	GFS	1.14 (JJA)	
	EPA (hourly)	No	Yes	GFS	1.86 (JJA)	
	EDGARv6 (monthly)	Yes	Yes	GFS	0.58 (JJA)	
	EDGARv6 (monthly)	No	Yes	GFS	1.24 (JJA)	
Martin Lake, TX (7 overpasses in JJA)	EPA (hourly)	Yes	Yes	GFS	1.29 (JJA)	
	EPA (hourly)	Yes	No	GFS	1.29 (JJA)	
	EPA (hourly)	No	Yes	GFS	2.27 (JJA)	
	EDGARv6 (monthly)	Yes	Yes	GFS	2.03 (JJA)	
	EDGARv6 (monthly)	No	Yes	GFS	3.34 (JJA)	

Table 1. A summary of the model-data slopes averaged over all simulations for each power plant. These values correspond to the horizontal lines in **Fig. 7** with removal of three "outliers" overpasses with significant wind directional biases. The results with the best configurations are outlined by solid black boxes. For the "no" NO_x chemistry simulation, a constant NO_2 -to-NO_x ratio is still applied.

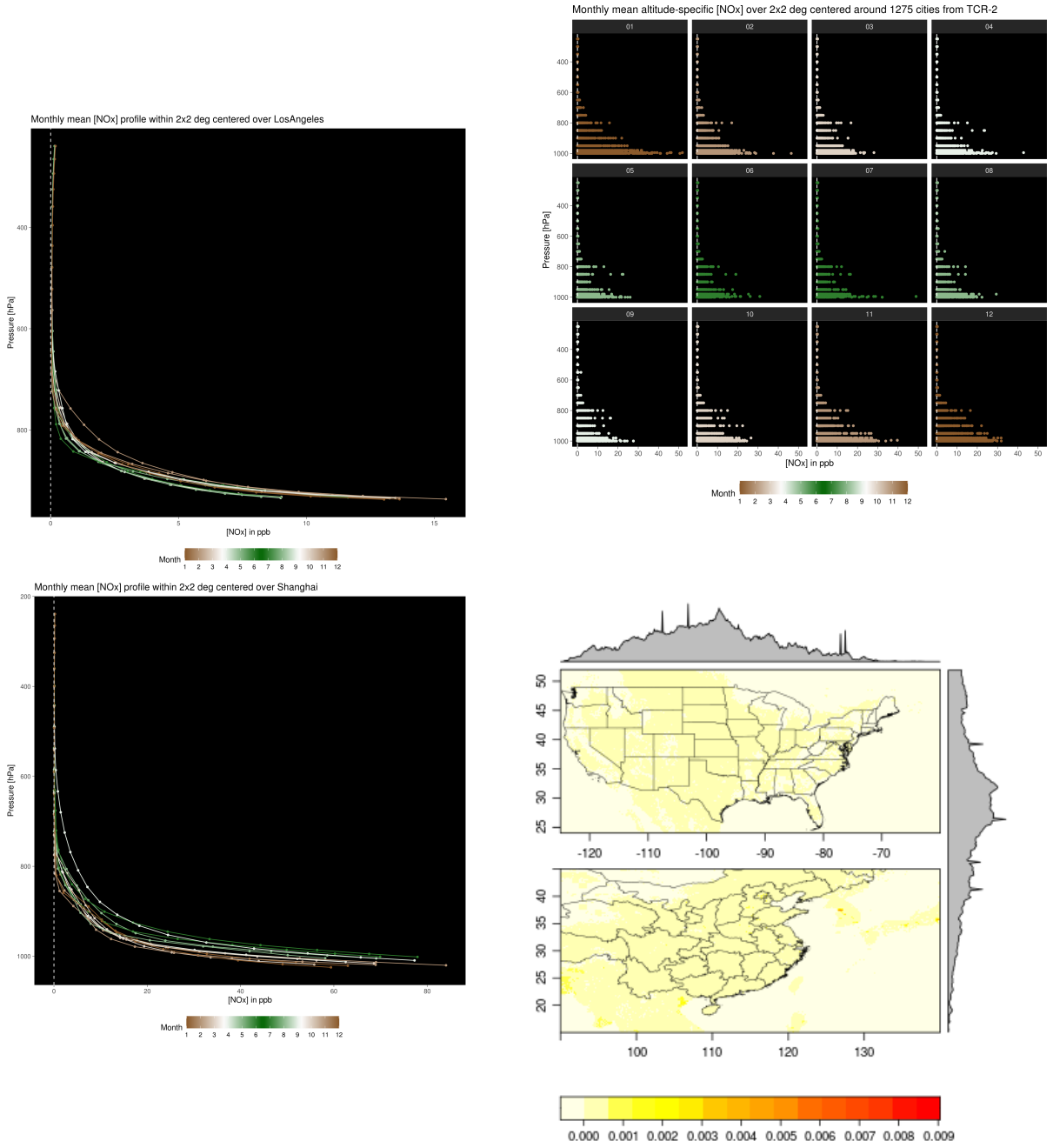


Figure S1. Left panels: monthly average level-specific NO_x mixing ratio [ppb] over 2° by 2° around Los Angeles (upper) and Shanghai (lower). WRF-Chem runs are driven by EDGAR emissions and generated for multiple selected days in a month. Upper right: month average pressure-specific NO_x mixing ratio [ppb] over 2° by 2° areas around thousands of global cities based on TCR-2 reanalysis in 2019. Each dot denotes one pressure level per city. The color gradient represents 12 months. Bottom right: Maps of non-anthropogenic NO_x emissions according to TCR-2.

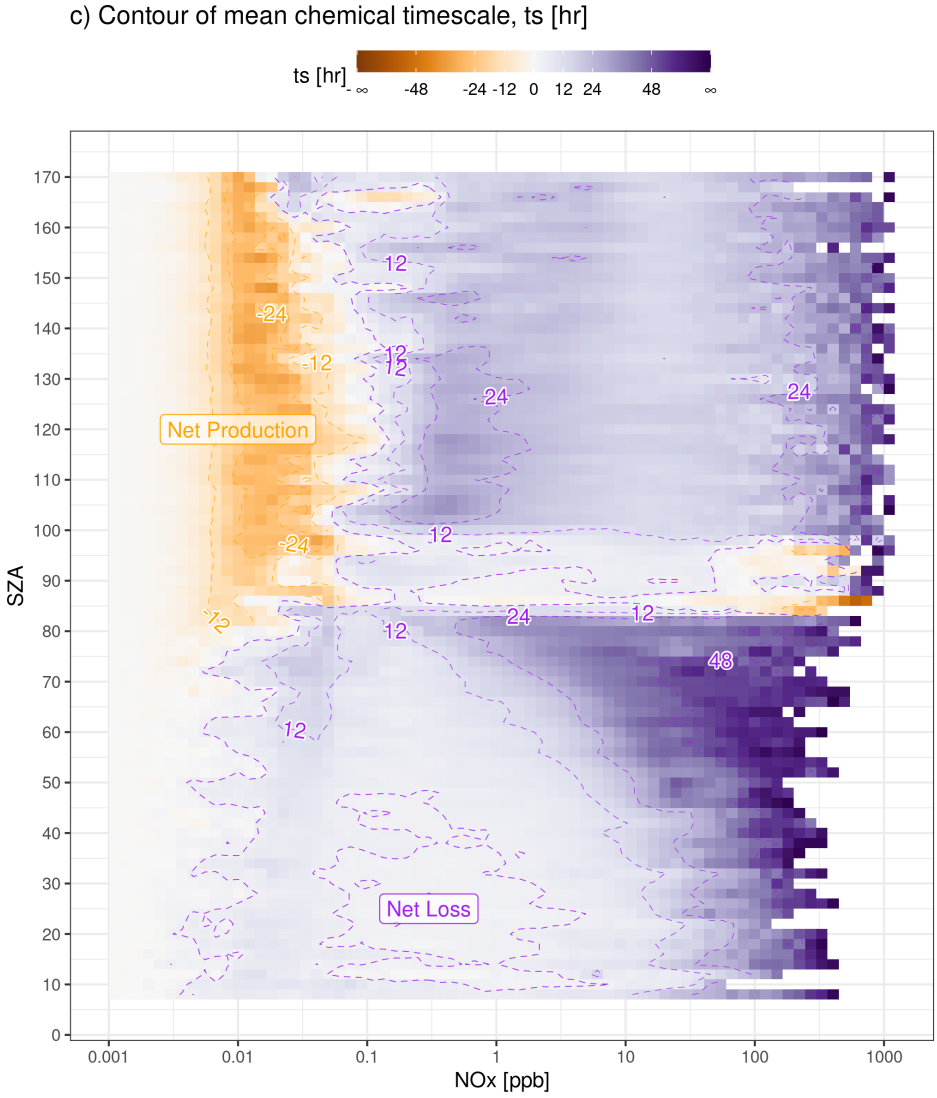


Figure S2. A contour view of the net NO_x loss timescale in hours, summarized for each SZA and NO_x bins, as an extension of Fig. 2b.

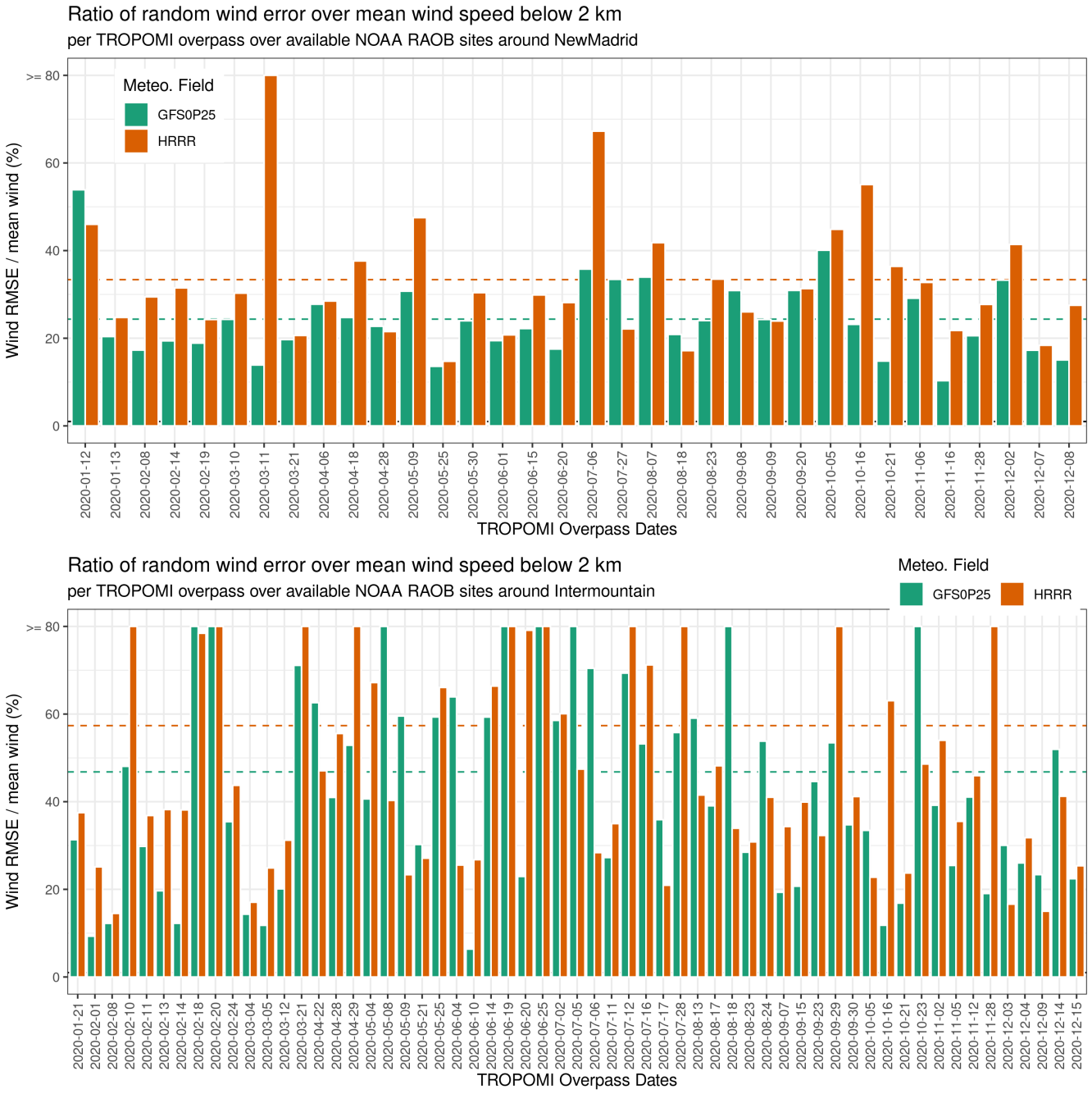


Figure S3. The modeled u-/v- component wind from 3km HRRR (orange bars) or GFS0p25 (green bars) are evaluated against measured wind speed from NOAA radiosonde sites based on all available observations around twp power plants, below 2 km during the 24 hours ahead of the TROPOMI overpass time. The random wind error normalized by the mean wind speed [%] is calculated for each overpass.

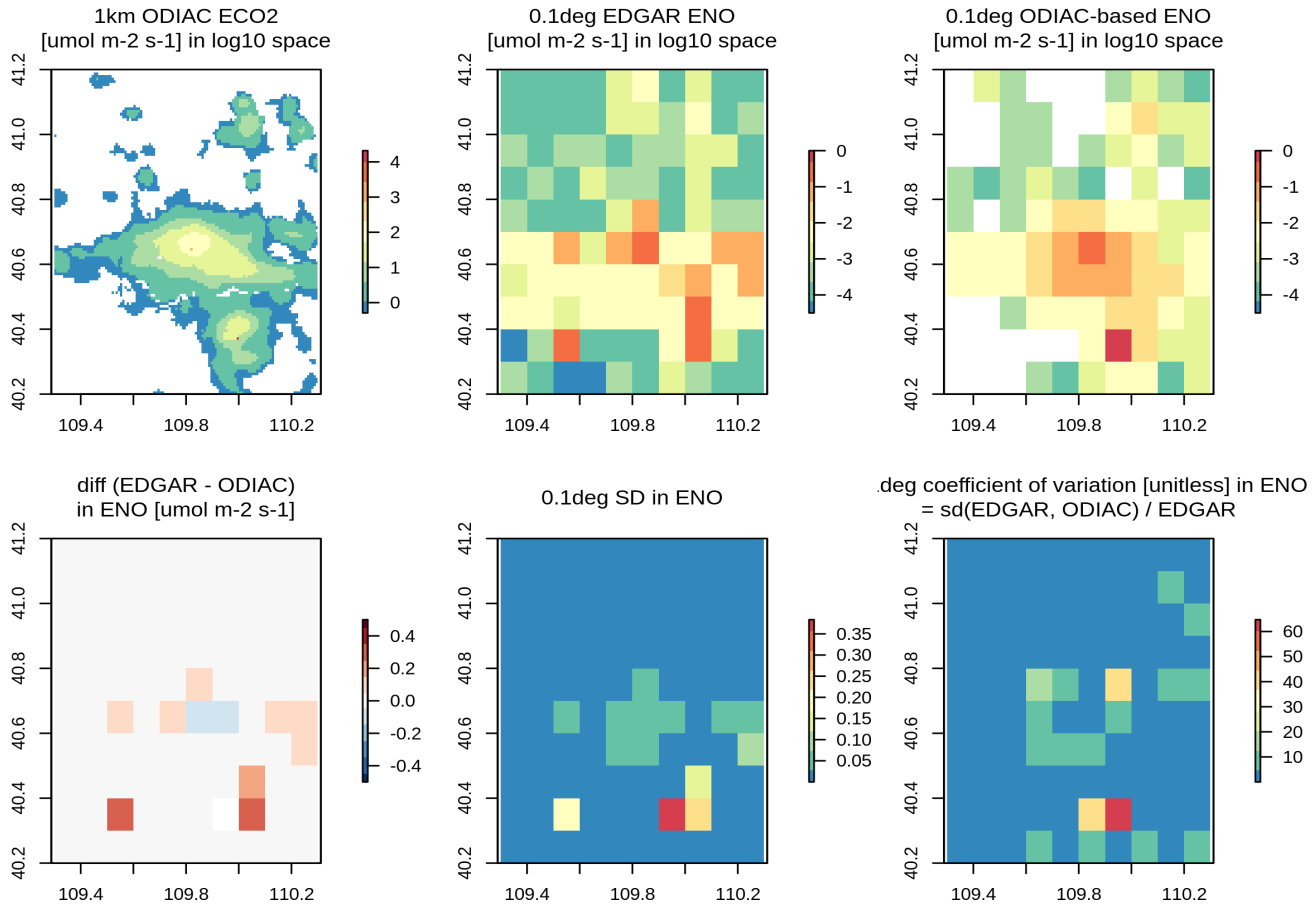


Figure S4. A demonstration of how prior emissions in NO_x can be approximated over Baotou, China. For example, we adopted the CO_2 emissions from ODIAC and the NO-to-CO_2 emission ratios from EDGAR to generate ODIAC-based NO_x emissions. The percent difference between the ODIAC-derived and EDGAR-based NO_x emissions can serve as prior emission uncertainty.

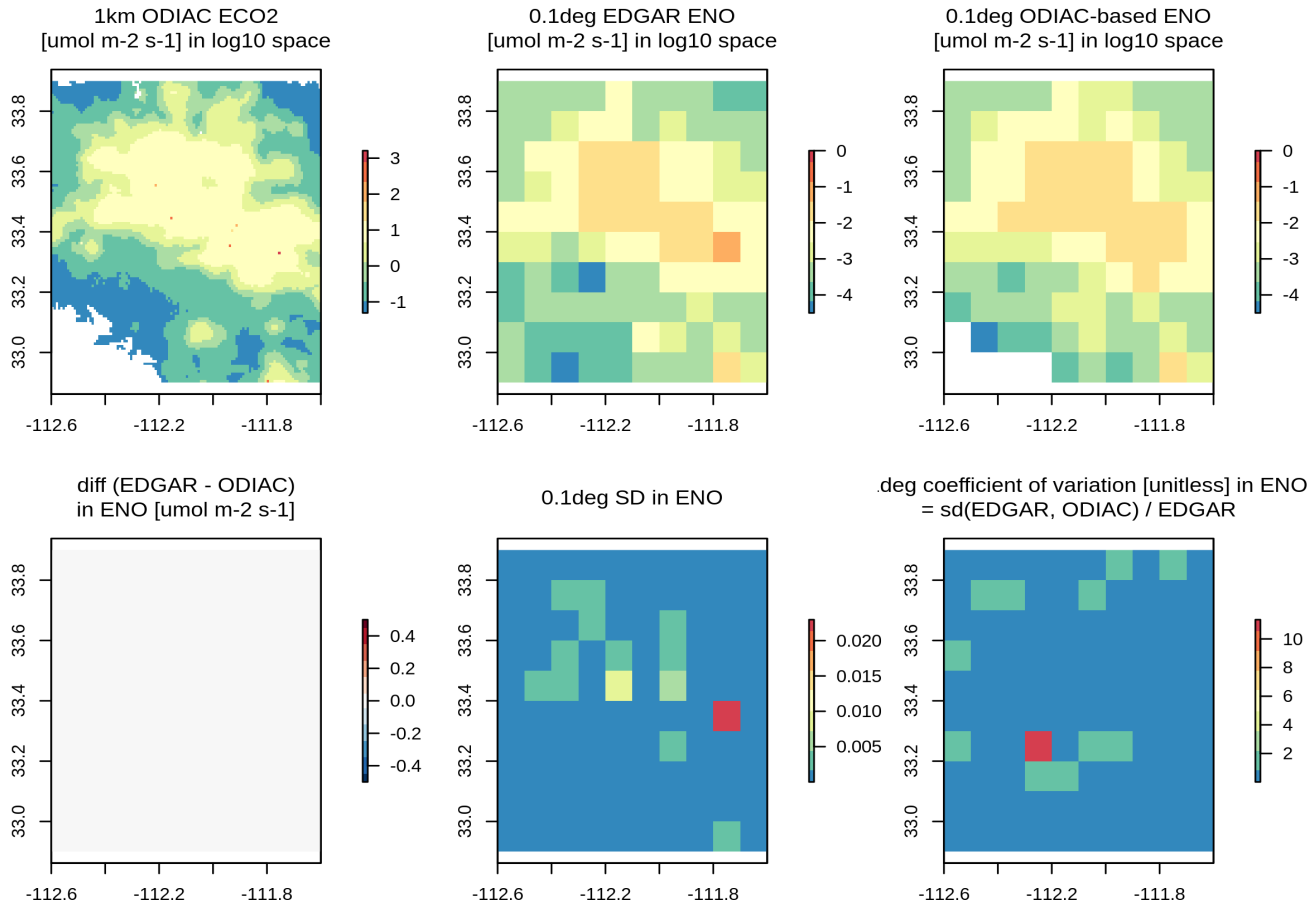


Figure S5. Same as **Fig. S4** but over Phoenix, USA. The prior uncertainty over Phoenix is much smaller than that over Baotou (**Fig. S4**).

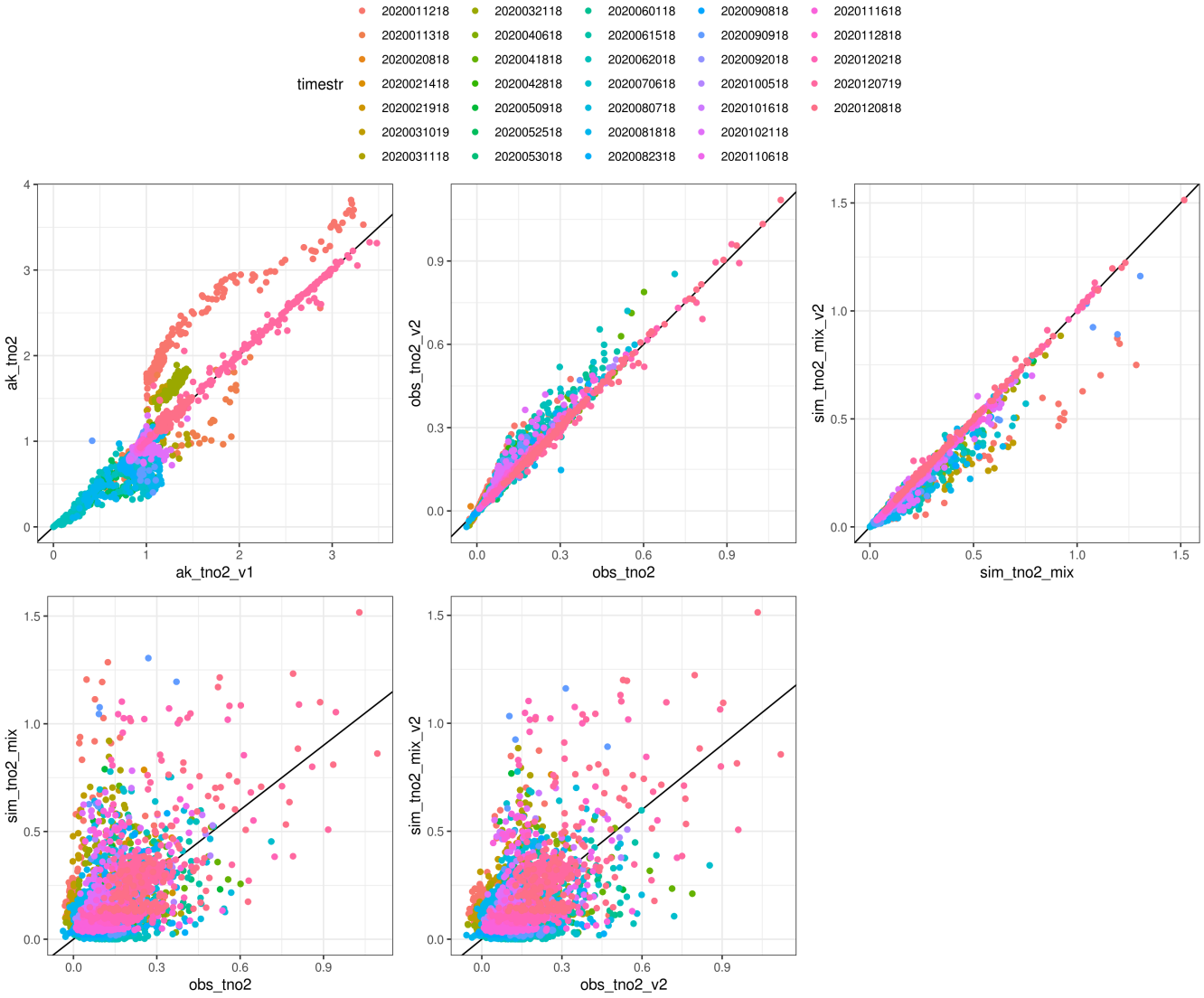


Figure S6. A summary of the differences between TROPOMI v1.3 and v2.3 over soundings around the New Madrid power plant for dozens of overpasses across seasons. Changes in the surface-level averaging kernel of tropospheric NO_2 [unitless], observed tNO_2 [ppb], simulated tNO_2 using version-specific AK profiles, and model-data comparisons between two versions are shown in each panel, respectively. Color differentiates overpasses and each dot represents one satellite sounding.

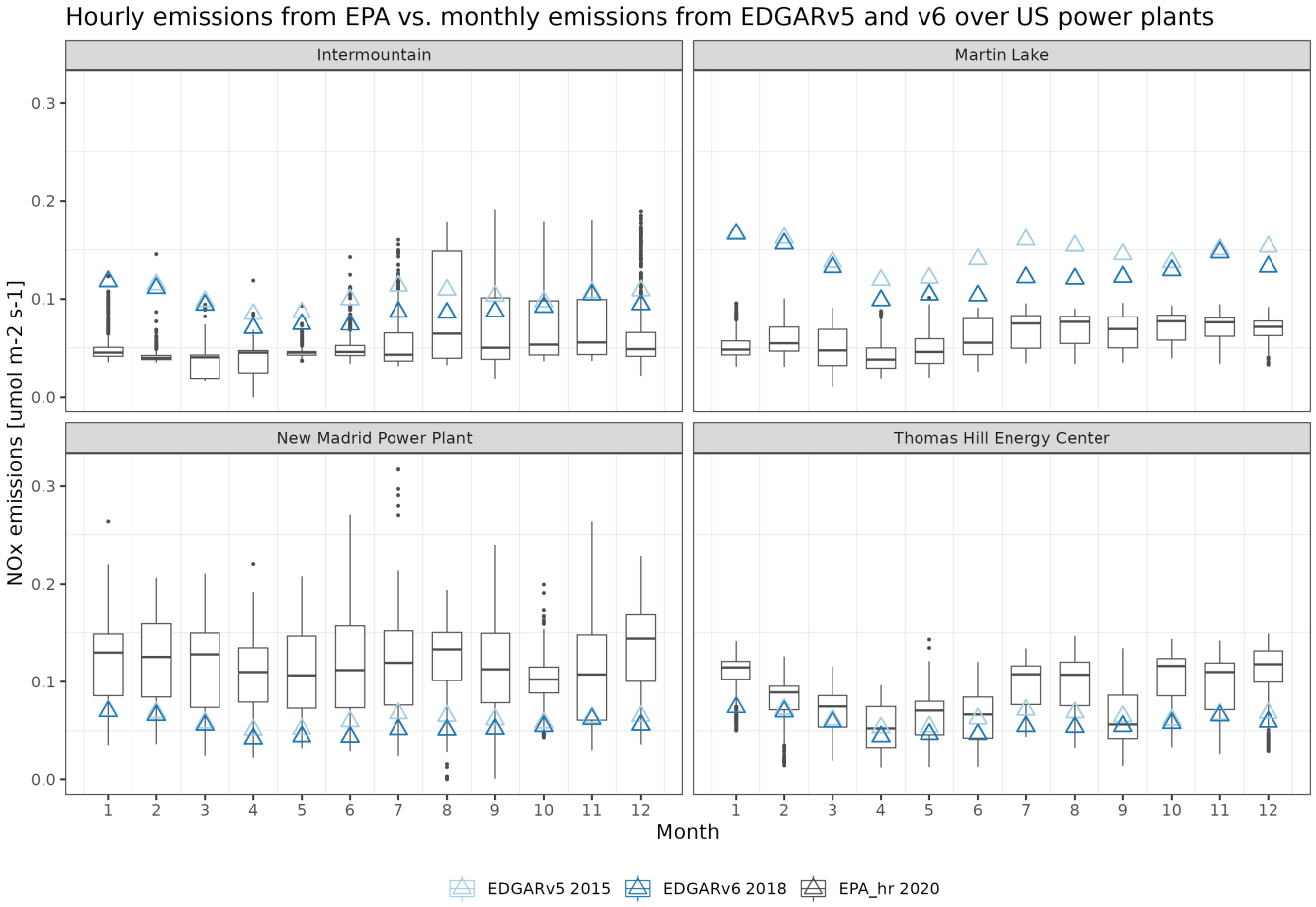


Figure S7. Reported hourly NO_x emissions in 2020 from EPA (black boxplot) [μmol m^{-2} s^{-1}] and monthly mean NO_x emissions from EDGARv5 (with the latest year available of 2015, light blue triangles) and v6 (with the latest year available of 2018, dark blue triangles) for examined power plants.

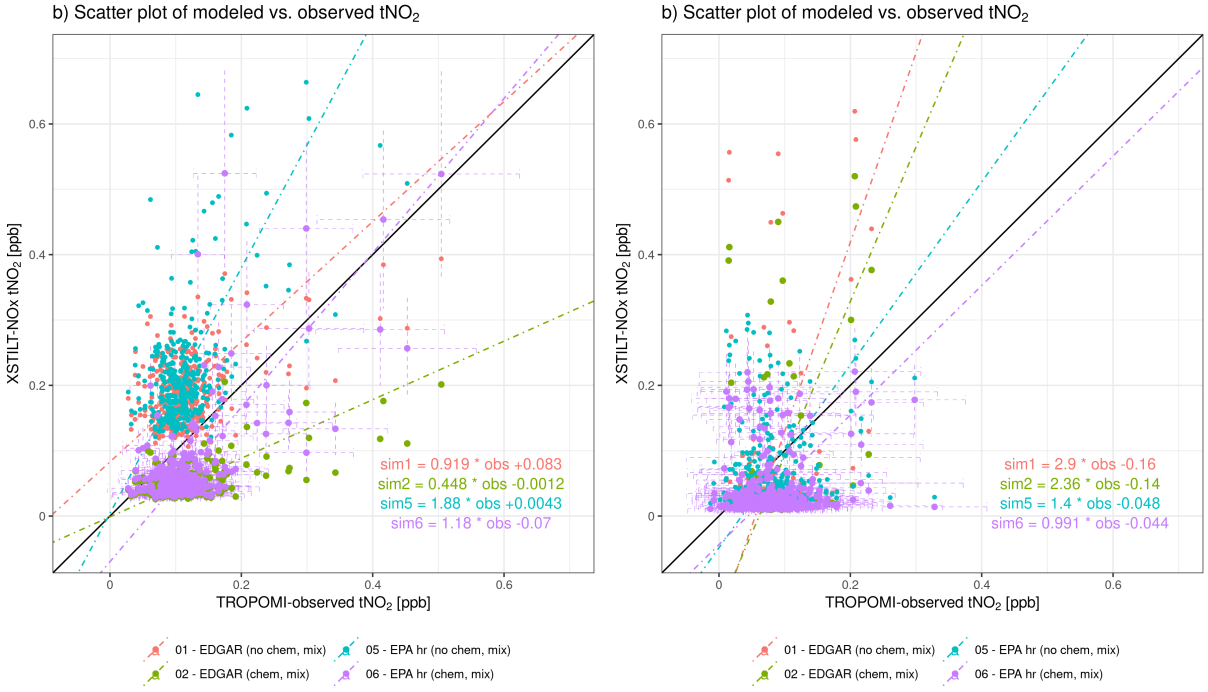


Figure S8. A scatter plot for the model-data comparison over the New Madrid power plant on June 15, 2020, and over the Intermountain power plant on Deb 14, 2020, based on TROPOMI v1.3 data. A similar comparison using TROPOMI v2.3 is presented in Fig. 6. Each dot denotes one satellite sounding. Only four GFS-based simulations using EDGAR without or with lifetime (red/green), and hourly EPA without or with lifetime (blue/purple) are included in the scatter plot. Linear regression fit with the Standardized Major Axis (SMA) solution is performed on the model-data pairs based on four select model configurations (dashed-dotted lines). The 1:1 line is displayed as a solid black line.

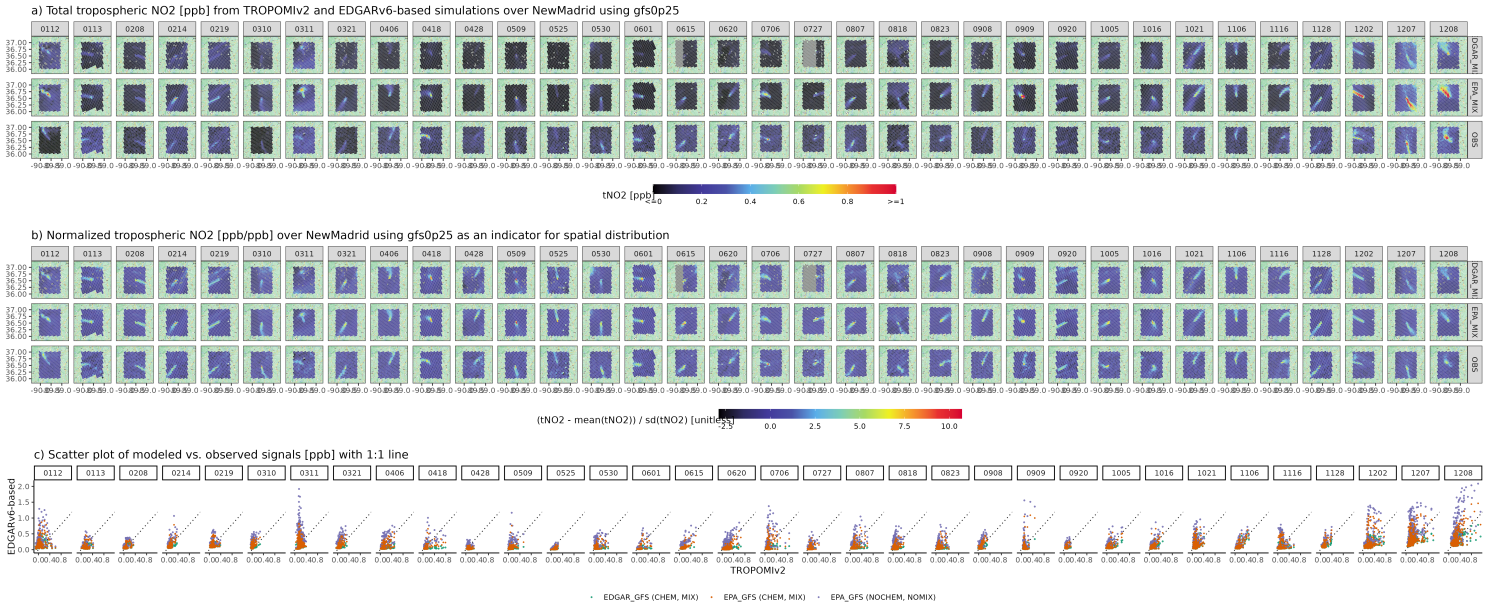


Figure S9. Model-data comparisons for all 34 overpasses around the New Madrid power plant using GFS0p25 as the meteorological field. Top panels: total tropospheric NO_2 from TROPOMIv2 and EDGARv6-based simulations. Middle panels: Standardized signals by first subtracting the spatial average and then normalized by the standard deviations (i.e., z-scores, [tNO2 - mean(tNO2)] / sd(tNO2), unitless). Bottom panels: Scatter plot of the model-data comparisons, including EDGARv6-derived simulations with NO_x chemistry (dark green) and EPA-derived simulations with (orange) and without NO_x chemistry (purple).

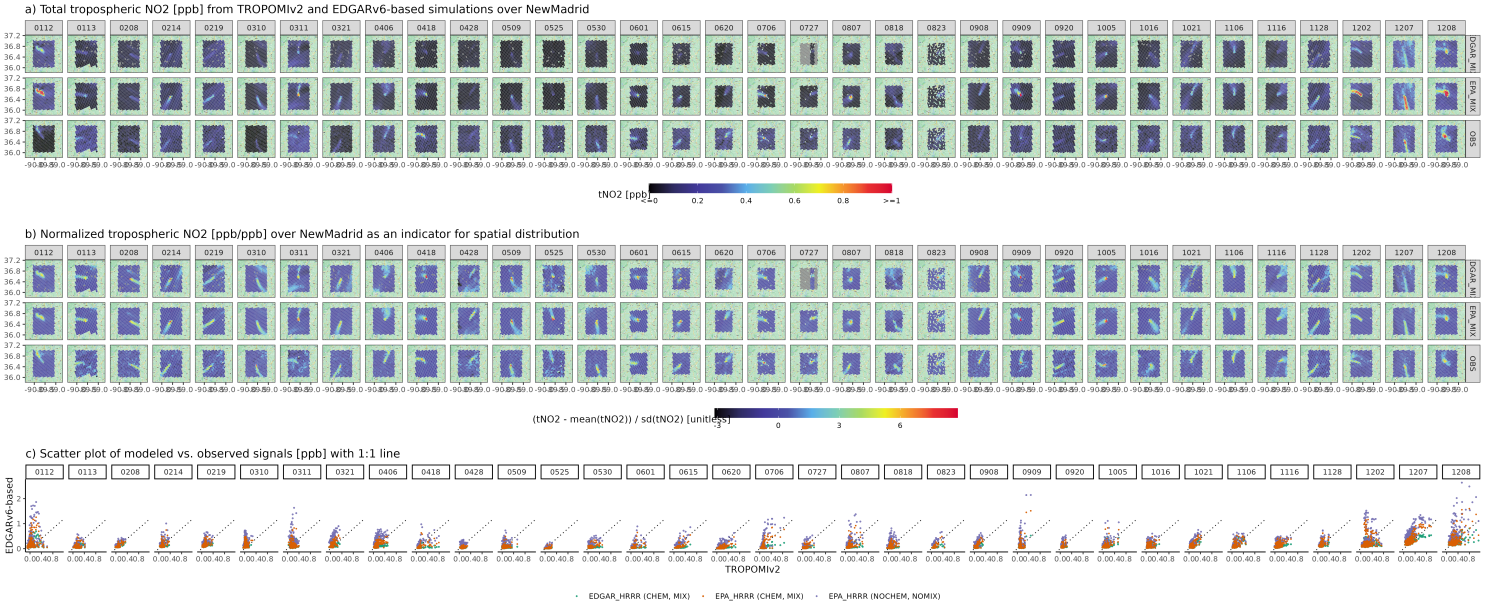


Figure S10. Same model-data comparisons as **Fig. S9** around the New Madrid power plant, but for simulations using HRRR as the meteorological field.

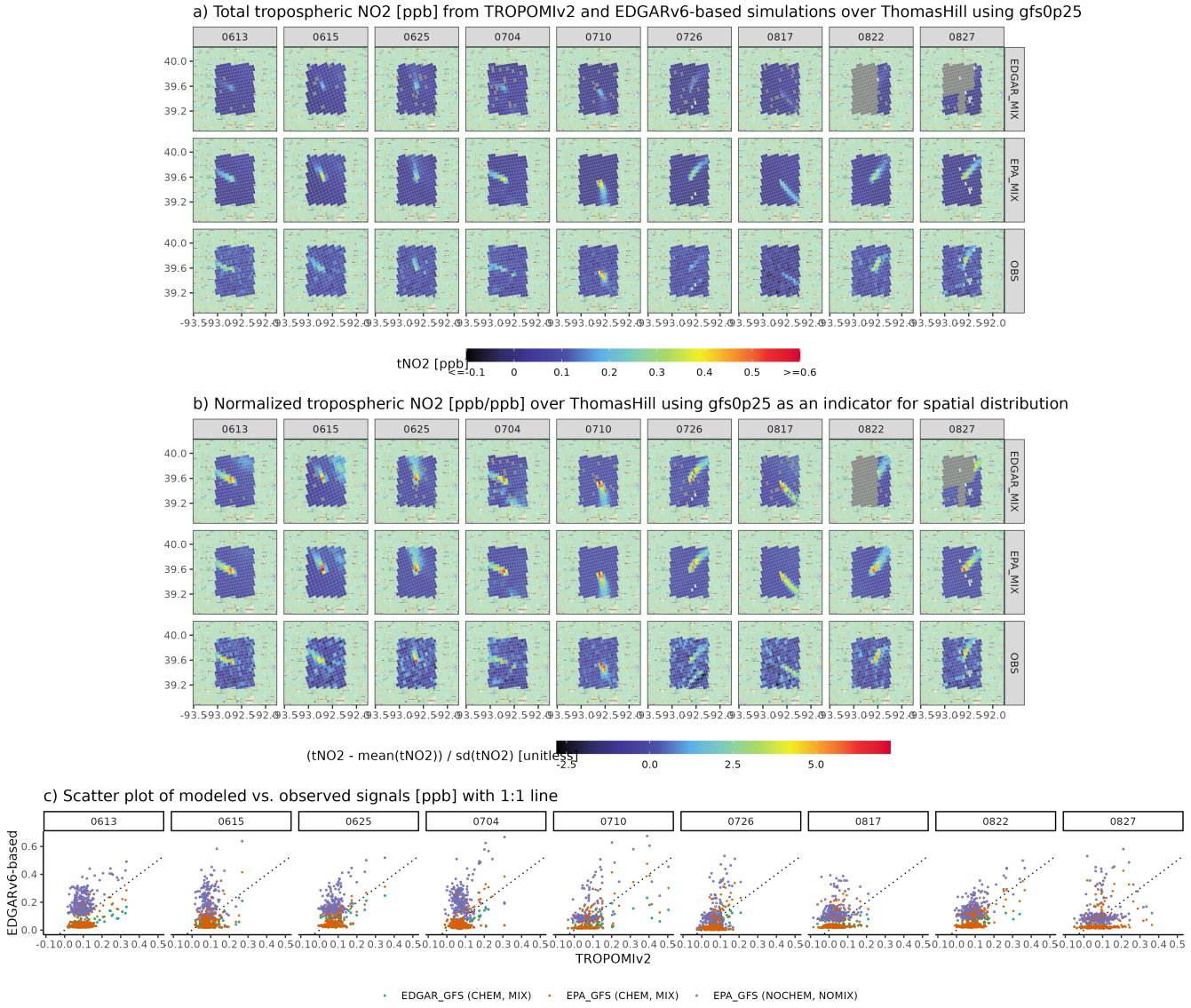


Figure S11. Same model-data comparisons as **Fig. S9**, but for simulations over the Thomas Hill power plant using GFS as the meteorological field.

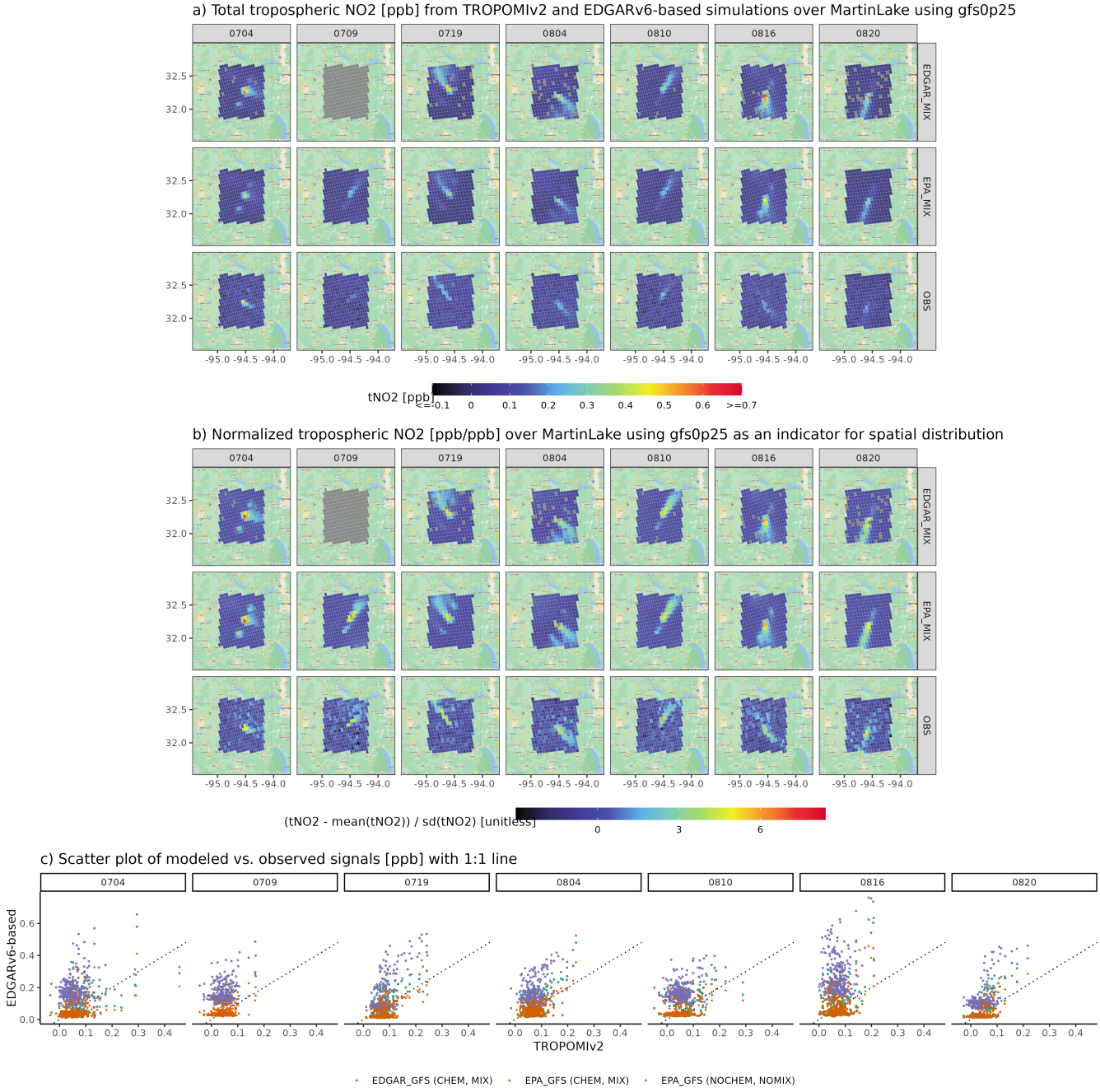


Figure S12. Same model-data comparisons as **Fig. S9**, but for simulations over the Martin Lake power plant using GFS as the meteorological field.

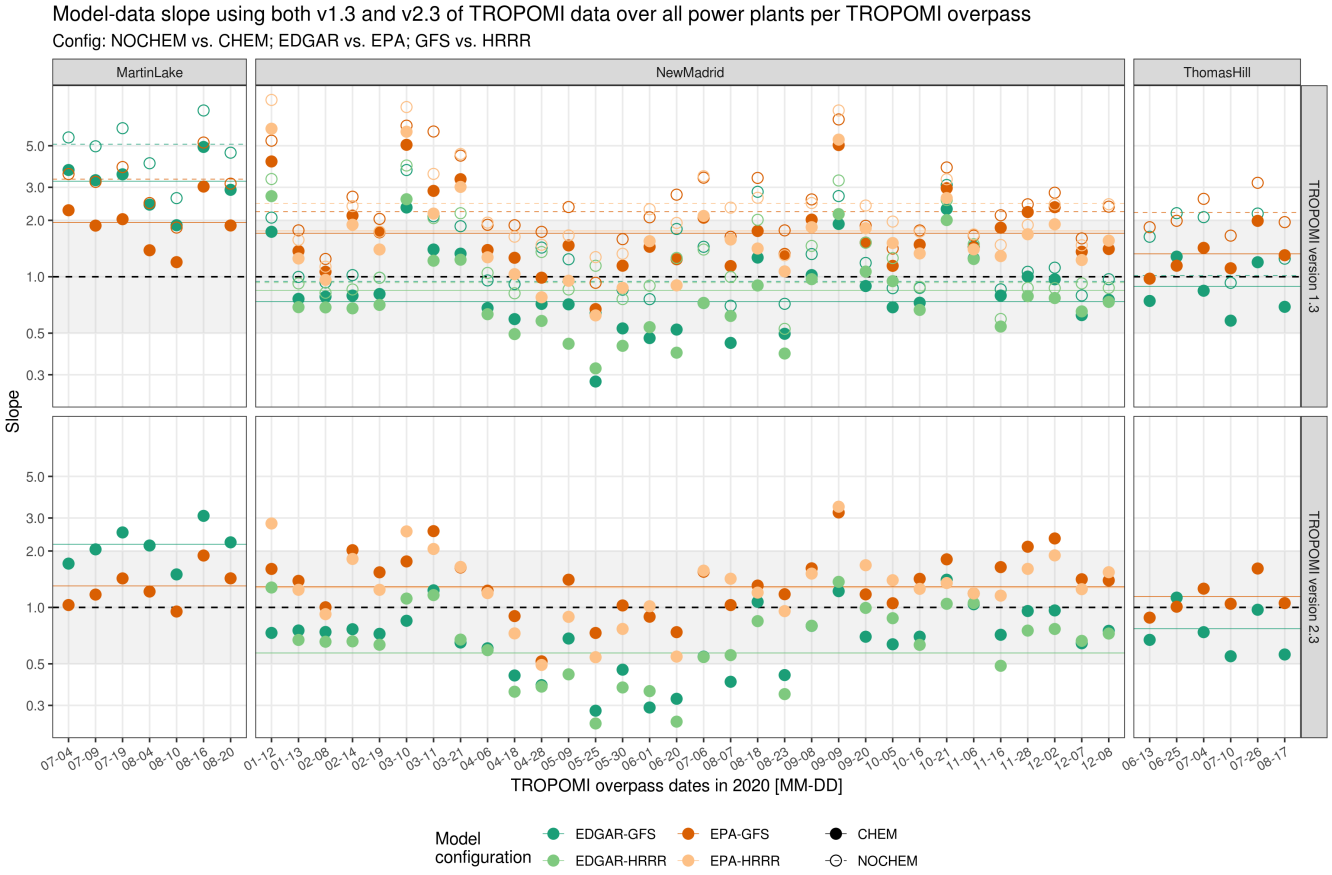


Figure S13. Same as **Fig. 6**, but the observations are obtained from both TROPOMI v1.3 and v2.3, while the simulations are carried out using annual mean EDGARv5.0 with the latest year available of 2015.

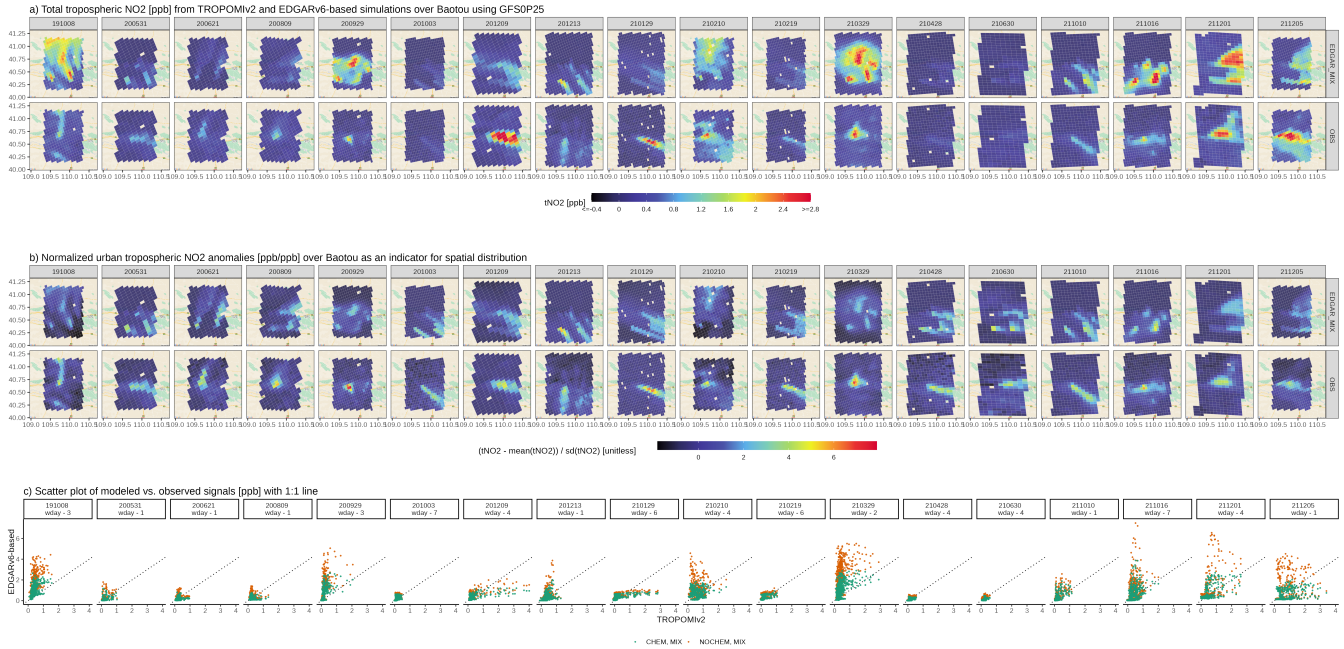


Figure S14. Examples of GFS/EDGARv6-derived and TROPOMIv2-based tNO_2 plumes over Baotou. Modeled plumes are generated using annual mean ENO_x from EDGAR with top emitters highlighted in light-grey circles. XCO_2 enhancements calculated from a local background have been averaged based on the TROPOMI sounding size. Only 18 TROPOMI overpasses that coincide with OCO-3 overpasses with time differences of < 1 hour are shown here.

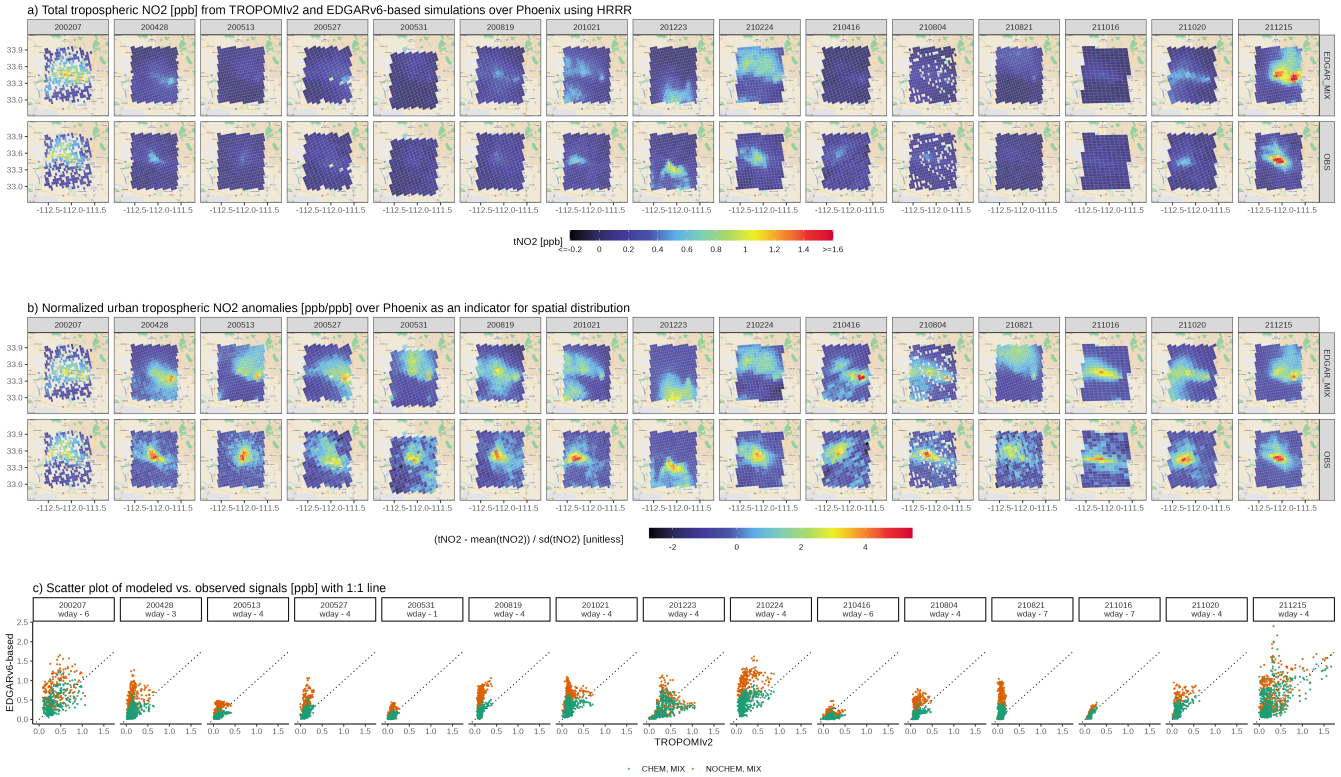


Figure S15. Same as **Fig. S14**, but over Phoenix. Only 15 TROPOMI overpasses that coincide with OCO-2 and OCO-3 overpasses with time differences of < 1 hour are shown here.

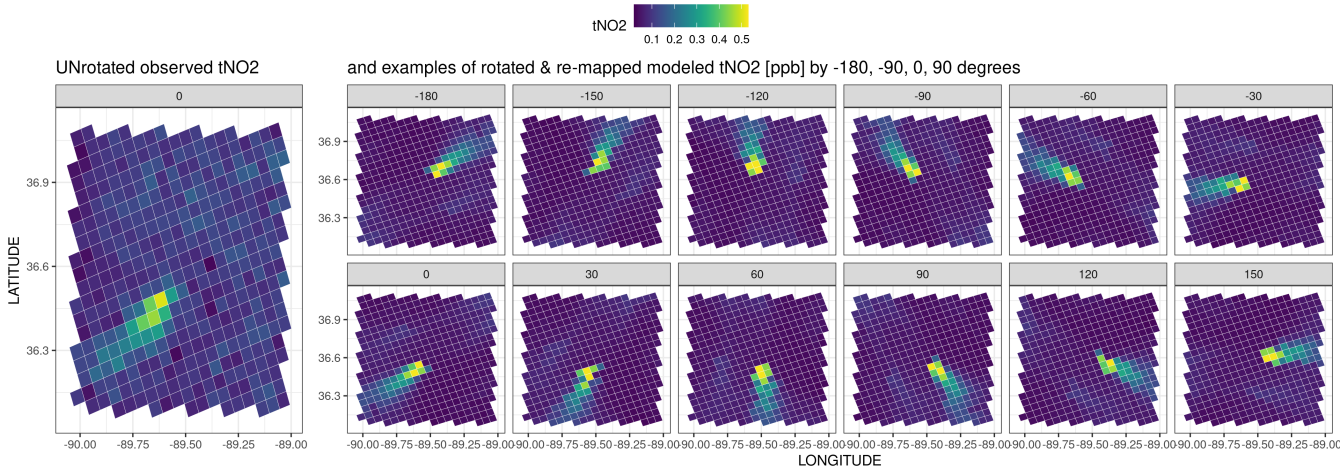


Figure S16. A demonstration of how modeled plume is rotated and re-mapped to the original TROPOMI pixels using $\mathrm{tNO_2}$ simulations on June 15, 2020, over the New Madrid power plant. Observed $\mathrm{tNO_2}$ on TROPOMI grids (upper left) and modeled $\mathrm{tNO_2}$ plumes with multiple rotation angles are plotted.

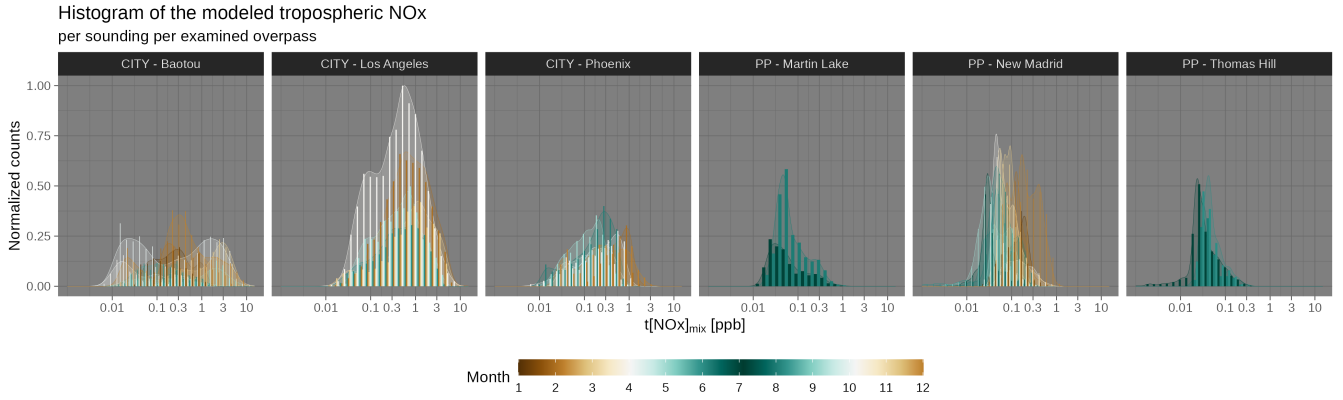


Figure S17. A histogram of the modeled tropospheric $\mathrm{NO_x}$ [ppb] for every TROPOMI sounding from all overpasses and all sites.

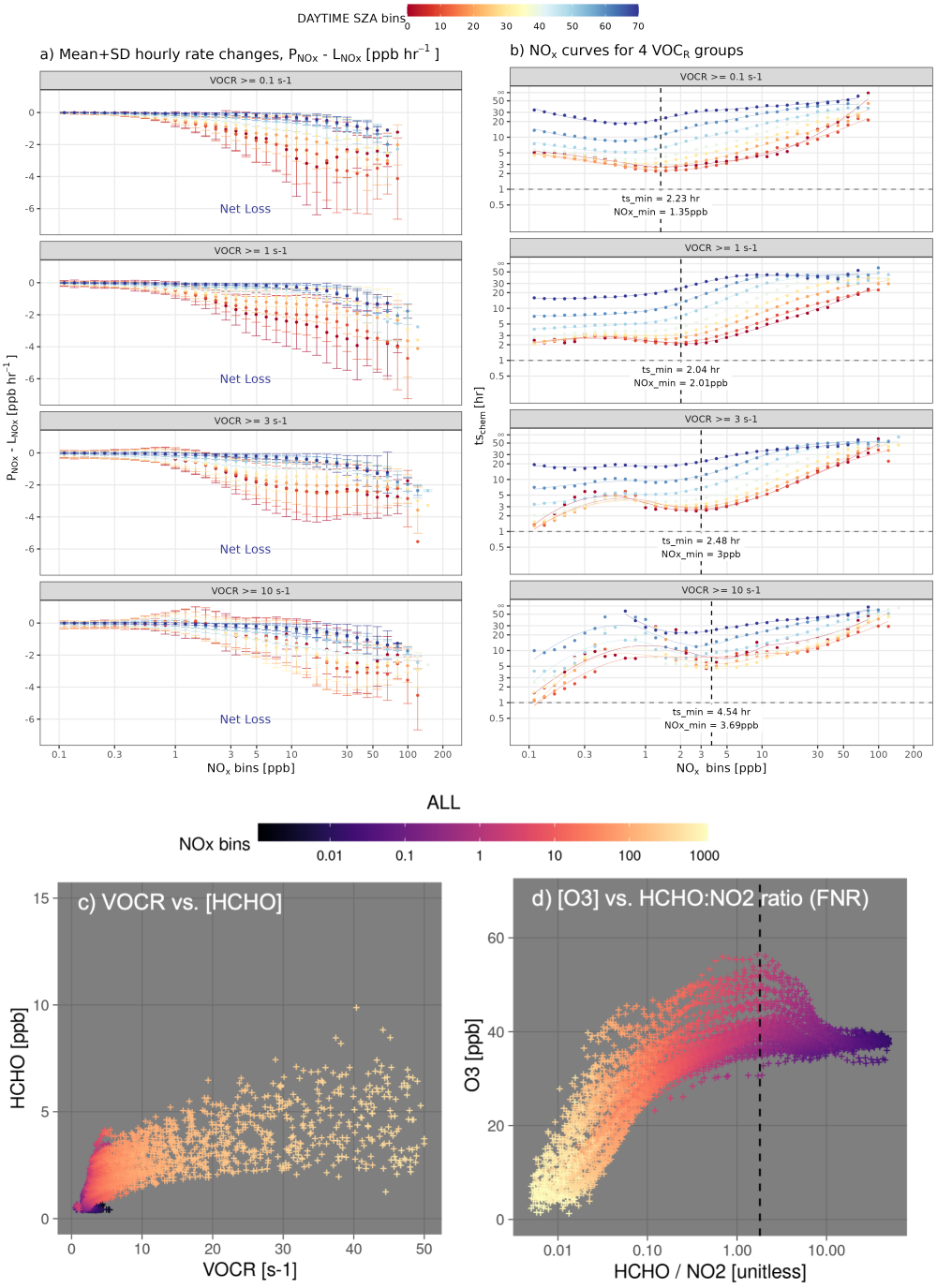


Figure S18. (ab) Similar to **Fig. 3ab**, but differentiated by three intervals of VOC_R and for selected SZAs intervals with a spacing of 10 degrees. All panels utilized model results from the same WRF-Chem simulations described in **Appendix A**. (cd) Relations of HCHO concentration [ppb] with VOC_R [s-1] and O_3 concentration [ppb] with HCHO:NO_2 ratio (FNR) with color gradient denoting modeled NO_x concentrations. All panels utilized model results from the same WRF-Chem simulations described in Sect. 2 and **Appendix A**.

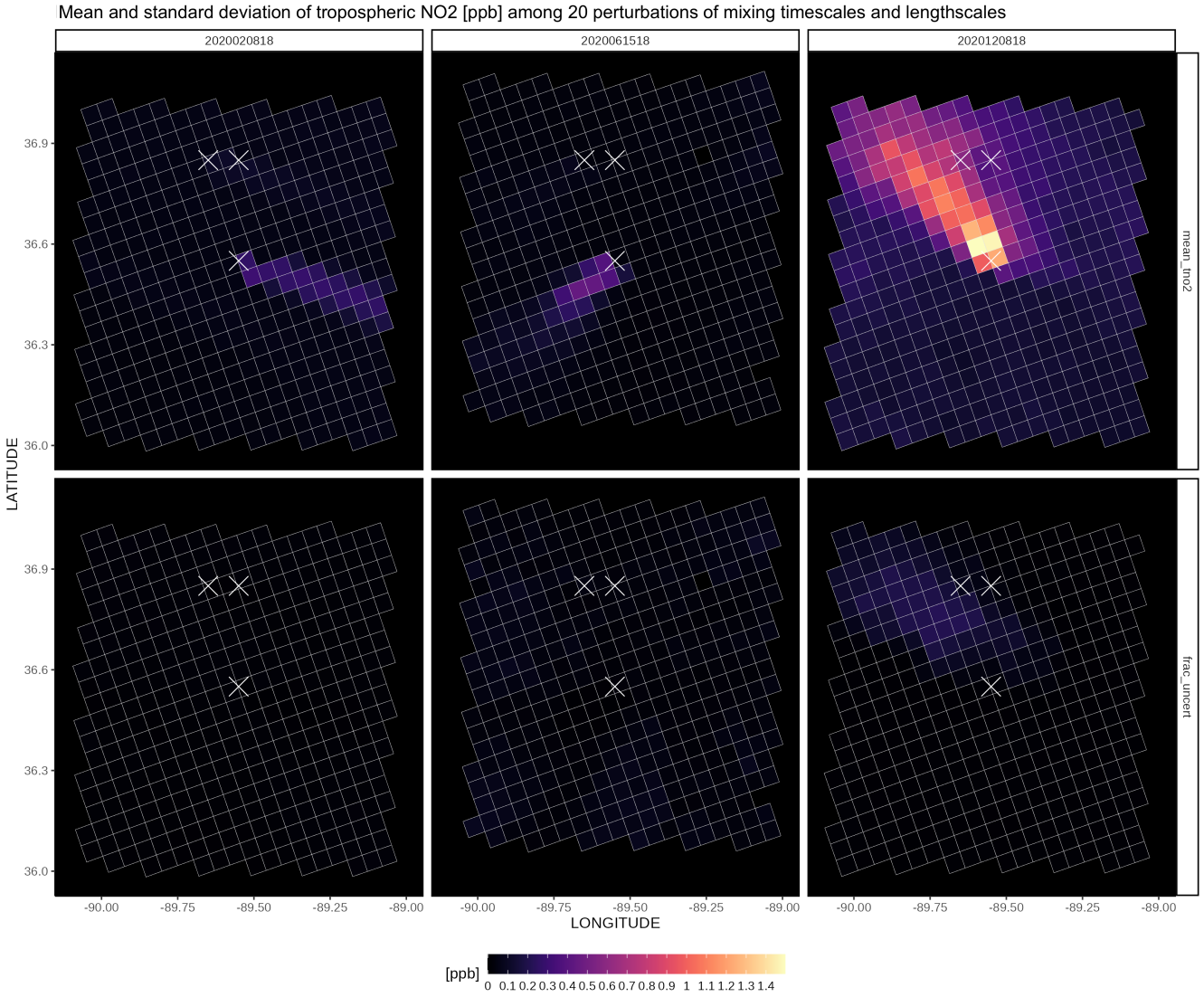


Figure S19. Mean and standard deviation of modeled tNO_2 for three TROPOMI overpasses (Feb 8, June 15, and Dec 8, 2020) over the New Madrid power plant using various horizontal mixing length scales (i.e., 0.5, 1, 3, 6, 12 km) and timescales (i.e., 0.5, 1, 6, 12 hours).